Optical nonlinearities in mixed type I–type II GaAs/AlAs multiple quantum wells

I. Galbraith

Department of Physics, Heriot-Watt University, Riccarton, Edinburgh EH14 4AS, United Kingdom

P. Dawson

Department of Pure and Applied Physics, University of Manchester Institute of Science and Technology, P.O. Box 88, Manchester M60 1QD, United Kingdom

C. T. Foxon

Department of Physics, Nottingham University, Nottingham, United Kingdom

(Received 9 July 1991)

We demonstrate all-optical nonlinearities at low cw pump powers (mW/cm^2) using a GaAs/AlAs double-quantum-well design that spatially separates photoexcited electron-hole pairs. The nonlinearities are examined over a range of temperatures and in a variety of samples. Theoretical calculations based on many-body interactions are in good agreement with the measured spectra and have been used to improve the structure design.

I. INTRODUCTION

Substantial progress in understanding and modeling the influence of a photoexcited electron-hole gas on the optical properties of semiconductor heterostructures has been made in the past decade.[1-3] Stimulated by the device potential offered by these materials, the absorption and refractive index changes produced by such a plasma have been intensively studied.[4] In this paper, we present the results of a systematic study of an asymmetric GaAs/AlAs mixed type-I–type-II double-quantum-well system which we have previously shown to exhibit very low power nonlinearities.[5,6] We investigate the barrier thickness and temperature dependence of the absorption spectra as well as the correlation between the saturation intensities and the characteristic recovery times of the bleached transmission. We also explore the temperature dependence of the nonlinear absorption.

The class of heterostructures which we investigate is shown schematically in Fig. 1. It consists of GaAs layers of thicknesses L_n and L_w forming two wells, separated by a barrier layer of AlAs of thickness L_b. These thicknesses are carefully chosen to ensure that the lowest electronic subband in each layer forms a "staircase" (see Fig. 1). The lowest electron state is localized at Γ in the wider GaAs layer, the second at the X minimum in the AlAs barrier, and the third, again at Γ, in the narrow GaAs layer. This arrangement necessitates the narrow well being type II with respect to the barrier, while the wider well is type I–hence our nomenclature "mixed type-I–type-II structures." Consider what happens to a photoexcited electron-hole pair generated above the band gap in the narrow well. The electrons in the narrow well thermalize, probably by scattering via the X state in the barrier, to form an electron plasma in the wide well. The transfer from Γ to X occurs typically on a subpicosecond time scale[7] and the subsequent X to Γ transfer should also occur on at most a submicrosecond time scale. The

lowest hole states in the two GaAs layers are essentially uncoupled, and at low temperatures holes are able to thermalize into the wider well only by tunneling through the AlAs barrier. If L_b is large the holes are effectively trapped in the narrow layer, thereby producing a very large spatial separation between the electron plasma and the hole plasma. Conversely, if the barrier is thin, the holes can easily tunnel into the wide well where they rapidly (≈ 300 ps) recombine with the electrons. Thus, the equilibrium carrier density generated by a given cw intensity will depend, via the hole tunneling time, on the barrier thickness.

Photons of sufficient energy to be absorbed in the narrow well can also be absorbed in the wide well. However,
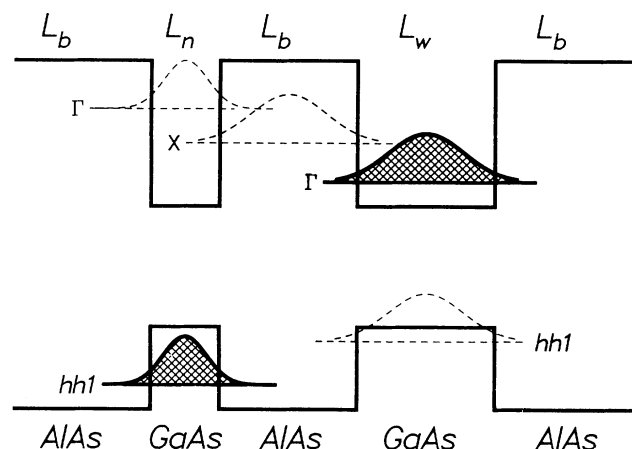

FIG. 1. Schematic diagram showing the conduction- and valence-band edges of the mixed type-I–type-II structure, illustrating the relative positions of the various confined electron and heavy-hole energy levels. The hatched regions indicate the photoexcited plasmas.

electron-hole pairs excited directly in the wide well recombine rapidly[8] at low temperatures ($\tau \approx 300$ ps) and therefore would not contribute appreciably to the equilibrium carrier density. This is demonstrated experimentally below. At room temperature the recombination time can be much longer, as it is dominated by free-carrier processes,[9] and thus carriers directly excited into the wide well may contribute significantly to the equilibrium carrier density. This is also investigated in more detail below.

Measurements on type-I GaAs/(Ga,Al)As quantum wells (QW's), in which the electron and holes are confined in the same layer, have been reported. At both room temperature[9,10] and low temperature[11-14] the heavy-hole excitonic resonance is shown to bleach strongly as the pump intensity is increased. No appreciable shift in the exciton peak energy is seen at moderate intensities. At sufficiently high pump intensities, a gain region appears below the absorption edge due to recombination in the photoexcited plasma. The changes in the absorption coefficient are accompanied by large changes in the refractive index. Theoretical work, which successfully describes this behavior in terms of many-body interactions within the electron-hole plasma, has also been extensively reported.[15-18] Several effects play an important role in such a theory. First, there are the mutual electron-electron, hole-hole, and electron-hole Coulomb interactions within the plasmas. These interactions are, in turn, screened[6] by the plasmas themselves. Second, there are the effects of the Pauli-exclusion principle. In it simplest form this is manifest as a blocking of absorption into occupied states. However, in systems where excitonic properties dominate the absorption edge, the Pauli principle also limits the electron and hole free-particle states which can intermix to give rise to the exciton. Third, a factor which arises from the antisymmetric nature of the fermion wave functions is the self-energy, which can be thought of crudely as a shift in the plasma resonances brought about by the exchange interaction. The consistent inclusion of exchange effects as well as screening of the Coulomb interaction and state filling are essential in reproducing the experimentally observed spectra.

Studies of room-temperature bleaching effects in electrically biased, type-I QW's have also been reported.[19] The saturation intensity (i.e., the intensity required to reduce the exciton absorption by 50%) is found to decrease with increasing barrier thickness and height, and increase with increasing electric field. This behavior correlates with changes in the time the electron-hole pair spends in the well and hence with the equilibrium carrier density maintained by the pump beam.

More recently type-II (Ga,Al)As/AlAs quantum wells have been investigated.[7,20-23] In type-II quantum wells there exists an electron state in the barrier region at lower energy than the lowest allowed electron state in the well. Consequently, an electron initially excited in the well will relax into the lower-energy barrier state. In the (Ga,Al)As/GaAs material system the lowest state in the barrier lies at the X point in the Brillouin zone, its exact nature, i.e., whether it is X_z or X_{xy}, depending on the barrier thickness.[24] At low temperature (15 K), a strong

blueshift of the lowest heavy-hole transition is seen for increasing pump intensity, accompanied by a slight redshift of the light hole.[20,22] The origin of the shifts again lies in the many-body interactions within the single-component hole plasma, and corresponding many-body calculations have been carried out.[20,25] Induced absorption on the low-energy side of the exciton also has been observed in a single beam saturation experiment and ascribed to space-charge effects.[23] One feature which distinguishes the type-II spectrum from the type-I spectrum is the absence of gain at high carrier densities. This is again attributable to the spatial separation of the electrons and holes.

Typically, one requires areal carrier densities of $\approx 5 \times 10^{11}$ cm^{-2} to achieve a significant change in the absorption coefficient. The equilibrium density generated by a cw intensity I at frequency $\hbar\omega$, with an absorption coefficient α and lifetime τ, is given by $n = \alpha \tau I / \hbar\omega$. At low temperature in type-I GaAs/AlAs QW's the exciton radiative lifetime is about 1 ns, hence cw intensities of ≈ 1000 W/cm^2 are needed. At room temperature, the recombination is dominated by free-carrier recombination and the lifetime can be much longer. Luminescence decay times may be as long as 500 ns and saturation intensities of ≈ 200 W/cm^2 have been reported.[9] In type-II structures, the spatial separation of electrons and holes and the Γ-X mixing for electron states increases the radiative lifetime to ≈ 1 μs at 10 K. This leads to a decrease in the cw intensity required to produce a given carrier density and hence allows nonlinearities to occur[6] at ≈ 10 W/cm^2. We shall show in this paper that in the mixed type-I–type-II structures, the limiting time can be many μs resulting in cw intensities as low as a few mW/cm^2 at 10 K.

In Sec. II we present the details of the samples and the experimental setup, in Sec. III we outline the theoretical calculations which support our experimental measurements, and in Sec. IV we present and discuss the results of our pump-probe spectroscopy and compare them with the calculations.

II. SAMPLES AND EXPERIMENTAL SETUP

The samples for this study were grown by molecular-beam epitaxy in a Varian Gen II machine at a substrate temperature of 630 °C using As$_2$ arsenic. Two sets of GaAs/AlAs mixed type-I–type-II structures were grown on n^+ substrates. The first set of samples consisted of nominally (a) 6800 Å of GaAs, (b) a 6000-Å-thick etch stop layer of Al$_{0.6}$Ga$_{0.4}$As, (c) a multiple-quantum-well region consisting of twenty periods of 25- and 50-Å GaAs double quantum wells separated by AlAs barriers 25, 42, and 76 Å thick in the different samples, (d) a 6000-Å-thick etch stop layer of Al$_{0.6}$Ga$_{0.4}$As, and (e) a 1000-Å-thick GaAs capping layer. In the second set of samples, the multiple-quantum-well region consisted of twenty periods of 25- and 68-Å GaAs quantum wells separated by AlAs barriers 76, 84, 93, and 103 Å thick in the different samples. The AlAs-layer thicknesses were measured by x-ray diffraction (XRD) for this second set of samples and are shown in Table I. The well thicknesses obtained from the XRD were within a monolayer of the

TABLE I. Sample barrier thicknesses L_b, saturation intensities I_s, and decay times $t_{1/2}, t_{Yu}$.

Nominal L_b (Å)	X-ray L_b (Å)	I_s (mW/cm^2)	$t_{1/2}$ (μs)	t_{Yu} (μs)
76	72	640	9.6	1
84	80	280	26	15
93	90	90	64	65
103	109	2.8	480	2000

nominal thicknesses. We use the nominal thicknesses as sample labels throughout this paper.

The mechanism responsible for the nonlinearities is carrier-carrier scattering and state filling within the photoexcited electron-hole plasma, and as such the plasma density is the key parameter. In order to vary the density controllably we use pump-probe absorption spectroscopy. This type of experiment consists of two distinct steps. First, carriers are excited by a variable power (usually cw) pump beam at a frequency above the band gap. Second, a weak probe beam measures the absorption spectrum of the excited sample.

The pump-probe absorption experiments were performed with the samples mounted on the cold finger of a variable temperature (4–300 K) continuous flow liquid-He cryostat. The samples were polished, etched, and mounted on sapphire disks to facilitate the optical transmission experiments. The samples were simultaneously illuminated by probe light from a chopped (100-Hz) tungsten lamp and a variable pump intensity from a cw or modulated dye laser operating at 1.97 eV. For the experiments which required a pump power density of greater than 10 W/cm^2, the laser was modulated to give 12-μs pulses at a repetition rate of 1 kHz to prevent sample heating. The transmitted probe light was analyzed by a 1-m grating spectrometer and detected by a cooled GaAs photomultiplier. The signal was processed by a lock-in detector referenced to 100 Hz to remove any luminescence created by the pump beam from the absorption spectrum. In the cases where the pump laser was modulated, the signal was also processed by a boxcar detector whose 0.5-μs gate was delayed during the pump pulse by an amount sufficient for the equilibrium carrier density to build up to its maximum value.

III. THEORY

As mentioned in the Introduction, calculations of the absorption changes in type-I and type-II quantum wells have been reported previously. In this paper, we perform essentially similar calculations to compute the effect of the electron plasma in the wider well on the absorption spectrum. We follow closely the work on the type-II nonlinearities, taking into account, where appropriate, the electronic nature of the plasma (as opposed to the holes in type-II samples[25]). We neglect coupling of light- and heavy-hole bands, performing the absorption calculation separately for each species.[26] The total spectrum is found by adding the heavy-hole spectrum plus one-third of the light-hole spectrum. This factor of one-third

reflects the symmetry of the underlying atomic orbitals involved in the absorption.[27]

To calculate the nonlinear absorption coefficient, we begin with the screened Hartree-Fock Hamiltonian,[2] neglecting any hole-hole interactions,

$$\mathcal{H} = \sum_{\mathbf{k}} E_{e,\mathbf{k}} a_{\mathbf{k}}^{\dagger} a_{\mathbf{k}} + \sum_{\mathbf{k}} E_{h,\mathbf{k}} b_{-\mathbf{k}}^{\dagger} b_{-\mathbf{k}}$$
$$+ \frac{1}{2} \sum_{\mathbf{k},\mathbf{q} \neq 0} V_s(\mathbf{q})[f_{e,\mathbf{k}-\mathbf{q}} a_{\mathbf{k}}^{\dagger} a_{\mathbf{k}} + (P_{\mathbf{k}-\mathbf{q}}^* b_{-\mathbf{k}} a_{\mathbf{k}} + \text{H.c.})] .$$

(1)

The single-particle energies $E_{e,\mathbf{k}}$, $E_{h,\mathbf{k}}$ are assumed to have parabolic masses m_e and $m_{h(l)}$. $a_{\mathbf{k}}, b_{\mathbf{k}}$ are the annihilation operators for electrons and holes, respectively. The $f_{e,\mathbf{k}}$ are the Fermi functions describing the distribution of electrons in their energy bands. $P_{\mathbf{k}}$ is the polarization and $V_s(\mathbf{q})$ is the Fourier transformed, quasi-two-dimensional, screened Coulomb potential.

The interaction Hamiltonian describing the coupling of the light to the polarization is, in the dipole approximation,

$$\mathcal{H}_{\mathcal{J}} = \sum_{\mathbf{k}} [d_{\mathbf{k}} E(t) a_{\mathbf{k}}^{\dagger} b_{-\mathbf{k}}^{\dagger} + \text{H.c.}] ,$$

(2)

where $E(t)$ is the optical field and $d_{\mathbf{k}}$ is the dipole moment which is assumed constant for this calculation.

Following the steps used to calculate the semiconductor Bloch equations,[2] we can calculate the generalized Wannier equation

$$(\hbar\omega - E_{e,\mathbf{k}} - E_{h,\mathbf{k}} - i\gamma + \Sigma_{\mathbf{k}})\chi_{\mathbf{k}}$$
$$= (1 - f_{e,\mathbf{k}}) \left[d_{\mathbf{k}} + \sum_{\mathbf{k}'} V_s(\mathbf{k} - \mathbf{k}')\chi_{\mathbf{k}'} \right]$$

(3)

for the polarizability $\chi(\hbar\omega) = \sum_{\mathbf{k}} d_{\mathbf{k}} \chi_{\mathbf{k}}$, and hence the absorption coefficient. A finite homogeneous linewidth γ is introduced to account for dephasing collisions. Within the single plasmon-pole approximation[2,12] the self-energy is given by

$$\Sigma_{\mathbf{k}} = \sum_{\mathbf{k}'} f_{e,\mathbf{k}} V_s(\mathbf{k} - \mathbf{k}') + \sum_{\mathbf{k}'} V_s(\mathbf{k}') - V(\mathbf{k}') ,$$

(4)

where

$$V_s(\mathbf{q}) = \left[\frac{V(\mathbf{q})}{\epsilon(\mathbf{q})} \right] F(\mathbf{q}) ,$$

(5)

$$\frac{1}{\epsilon(\mathbf{q})}=1-\frac{1}{1+\dfrac{|\mathbf{q}|}{\kappa F(\mathbf{q})}+\dfrac{\hbar^2 v_{\mathbf{q}}^2}{\hbar^2\omega_{\mathrm{pl}}^2}}\ ,\tag{6}$$

with $\hbar^2\omega_{\mathrm{pl}}^2=(2\pi e^2/\epsilon_0 m_e)n|\mathbf{q}|F(\mathbf{q})$; $\hbar^2 v_{\mathbf{q}}^2=(\hbar^2 q^2/2m_e)^2$; $\kappa=2m_e e^2/\epsilon_0\hbar^2(1-e^{-\pi\hbar^2 n/m_e kT})$. n is the two-dimensional electron density and T the plasma temperature. $V(\mathbf{q})$ is the unscreened two-dimensional Coulomb potential. This approximation to the dielectric function has been shown to be a good approximation at low temperatures (30 K) in type-II quantum wells.[25] Use of this screening function limits our comparison with experiments to the low-temperature regime, as it is well known that neglecting the dynamical aspects of the screening function gives rise to anomalous redshifts due to an overestimate of the screening.

The form factor $F(\mathbf{q})$ represents the deviation of the Coulomb potential from a perfect two-dimensional potential,

$$F^{ij}(\mathbf{q})=\int dz\int dz'|\phi_i(z)|^2|\phi_j(z')|^2 e^{-|\mathbf{q}||z-z'|}\ .\tag{7}$$

The superscripts indicate that, strictly speaking, the electron-electron and electron-hole interactions are different. However, if the electron and hole remains well confined by the heterostructure, it is a good approximation to take $F(\mathbf{q})$ corresponding to an infinite well of thickness L. In this case, the confined electron and hole envelope functions are identical, yielding

$$F(\mathbf{q})=\frac{8}{q^2 L^2+4\pi^2}\left[\frac{3|\mathbf{q}|L}{8}+\frac{\pi^2}{|\mathbf{q}|L}\right.$$
$$\left.-\frac{4\pi^4(1-e^{-|\mathbf{q}|L})}{q^2 L^2(q^2 L^2+4\pi^2)}\right]\ .\tag{8}$$

We have verified this approximation for our structures by comparing Eq. (8) with a numerical evaluation of Eq. (7) for the realistic structure including finite barriers and effective-mass mismatches.

We solved Eq. (3) by discretizing the $\mathbf{k}$ points on four Gaussian quadrature intervals and solving the resulting set of (typically 90) linear equations numerically. The quadrature intervals were altered depending on the density and frequency in order to give an accurate representation of the matrix diagonal. In particular, points were concentrated around the $\mathbf{k}$ values where the diagonal elements changed sign. The cutoff wave vector was typically $32/a_0$, where a_0 is the bulk Bohr radius. The equilibrium electron density n is an input to the calculation and defines the chemical potential. The hole density is assumed to be zero for the purpose of the calculation.

The inhomogeneous broadening arising from well-width fluctuations makes a significant contribution to the measured absorption linewidth. We include this effect phenomenologically by averaging the computed homogeneous spectrum over a Gaussian distribution of well widths. The Gaussian distribution width is then varied to fit the measured *linear* spectrum and thereafter kept constant as the density increases.

IV. RESULTS AND DISCUSSION

A. Low-temperature results

As we mentioned in the Introduction, the interesting feature of these mixed type-I–type-II structures is that they optically create a population of long-lived, spatially separated electrons and holes, which enables us to observe nonlinear absorption changes at low pump power densities. We anticipate that the controlling factor (at 10 K) determining the magnitude of the equilibrium carrier densities will be the heavy-hole tunneling rate. Initial evidence for this behavior was provided by the behavior of the first set of samples with the 25- and 50-Å quantum wells.[5,6] We discuss first the experimental results for the 76-Å barrier sample. The absorption spectra around the 50-Å direct band edge for a variety of pump intensities are shown in Fig. 2. The linear spectrum shows heavy- and light-hole excitonic peaks, whose energies are in accord with envelope function calculations for a 50-Å quantum well. As can be seen, there is a clear shift in the absorption peaks to higher energies for both the $n=1$ heavy- and light-hole excitons as the pump intensity is increased. The light-hole resonance is somewhat broadened by an underlying Fabry-Pérot fringe which can be clearly seen on a wider range spectrum. At the highest pump power, the heavy-hole resonance shifts by 8 meV to higher energy and bleaches to 50% of its strength. The light-hole exciton shifts by slightly less and also bleaches. (The Fabry-Pérot interference makes it difficult to be quantitative about the light-hole shift in this sample.) It is noteworthy that the pump powers re-
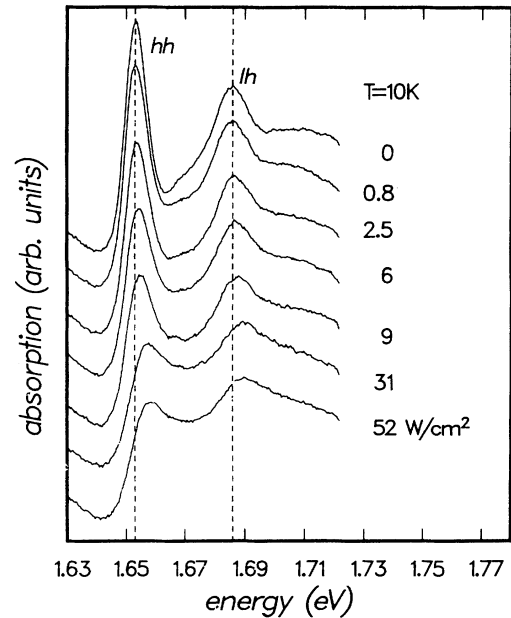

FIG. 2. Absorption spectra around the 50-Å QW band gap in the $L_n=25$ Å, $L_b=76$ Å, $L_W=50$ Å sample at various pump intensities. The spectra have been offset vertically for clarity. The pump energy is 1.95 eV, i.e., above the 25-Å QW band gap.
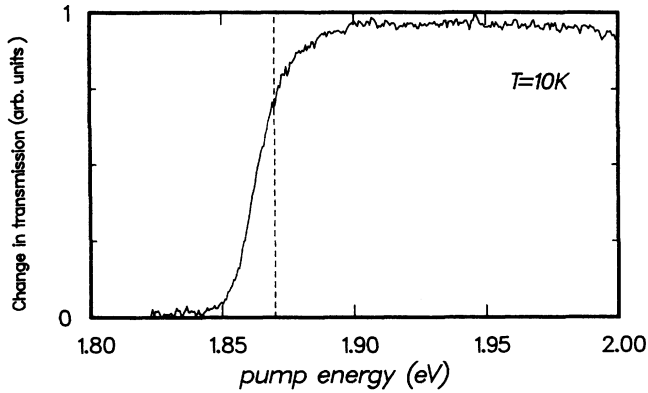
FIG. 3. Transmission change about the 50-Å QW band edge in the $L_n = 25$ Å, $L_b = 76$ Å, $L_W = 50$ Å sample as the pump energy is tuned through the 25-Å QW band gap.

FIG. 4. As Fig. 2, but spectrum around the 25-Å QW band gap.

quired to produce these effects are two to three orders of magnitude lower than those in conventional type-I quantum-well structures.[14] This we attribute to the long lifetime of the spatially separated carriers.

A particular feature of these structures is that the spatially separated carrier population, and hence the observed low power nonlinearities, can only arise if the energy of the pump light is above the 25-Å quantum-well band edge. This is demonstrated in Fig. 3, where the change in the transmission at the peak of the $n = 1$ heavy-hole exciton in the 50-Å well is shown as a function of the pump energy. As can be clearly seen, there is no change in transmission for pump energies below the 25-Å quantum band edge and a sharp onset as we tune across the gap (dashed line). This demonstrates the crucial point that the carriers created by the pump beam directly in the 50-Å well are insufficient in themselves to cause the bleaching.

The bleaching of the 50-Å quantum-well transitions is caused by the photoexcited electron plasma. The presence of a hole plasma in the 25-Å well also causes a bleaching around the 25-Å band edge, as can be seen in Fig. 4. This effect is essentially identical to the bleaching observed in wholly type-II quantum wells. The $n = 1$ heavy-hole exciton peak is rather broad as well-width fluctuations cause significantly more inhomogeneous broadening than in the 50-Å quantum-well spectrum. Nevertheless, a clear blueshift of the heavy-hole resonance can be seen. One also expects, as in the type-II structures, a slight redshift of the light-hole resonance. Unfortunately, our pump laser was unable to pump above the light-hole resonance and so this shift was not observed.

The experimentally observed bleaching appears to saturate at the highest pump powers used. We believe this is due to the periodic space-charge field set up by the alternating layers of electron and hole plasmas which will alter the conduction- and valence-band edges within the structure. The alignment of the subband levels in different layers of the structure is strongly affected by the space-charge potential. This in turn has an influence on
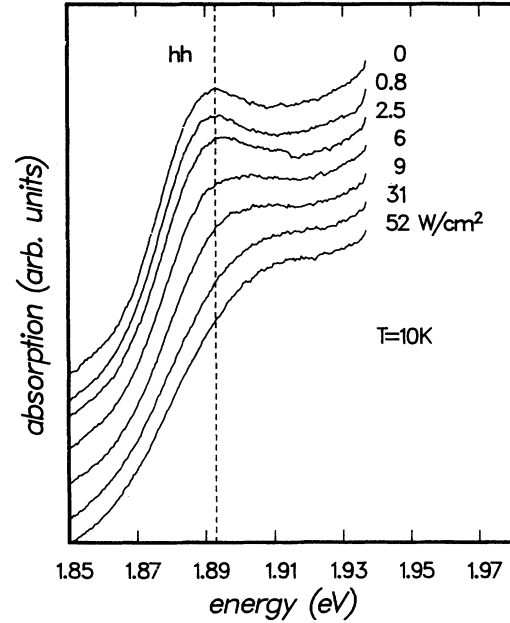
interwell processes such as indirect recombination[26] or the tunneling times between the wells.

With no carriers present, the $n = 1$ heavy-hole level in the 25-Å well lies about 30 meV below the $n = 2$ heavy-hole subband energy in the 50-Å well. The effect of the finite space-charge potential is to raise the energies in the 50-Å well relative to the 25-Å well. Thus, at a sufficient carrier density, the space-charge field can bring the $n = 2$ heavy-hole subband edge of the 50-Å well into resonance with the $n = 1$ subband edge of the 50-Å well. This will lead to a decrease in the time required for holes to tunnel from the 25-Å well into the 50-Å well. Upon reaching the 50-Å well they can recombine rapidly with the electrons in the plasma. Hence increasing the pump intensity produces ever smaller increases in the equilibrium carrier density. To check this idea quantitatively we have carried out a simultaneous solution of the Schrödinger-Poisson equation to find the subband energy levels in the periodic structure (see Ref. 25 for details). The results, as shown in Fig. 5, confirm that at an equilibrium carrier density of 5×10^{11} cm^2 there is sufficient potential difference to align the heavy-hole $n = 1$ subband in the narrow well with the heavy-hole $n = 2$ in the wider well. The carrier density used for this calculation is sufficient to produce the observed nonlinearities, as will be discussed later.

We note that the absorption process involves creation of an electron-hole pair in the same well and that the space-charge shift of the valence- and conduction-band edges are the same. In our multiple well structures the space charge is periodic, and within each quantum-well region it is essentially symmetric. Since the confinement energy is larger than the change in space-charge potential within the well, one can neglect the influence of the space charge on the direct absorption edges in the many-body
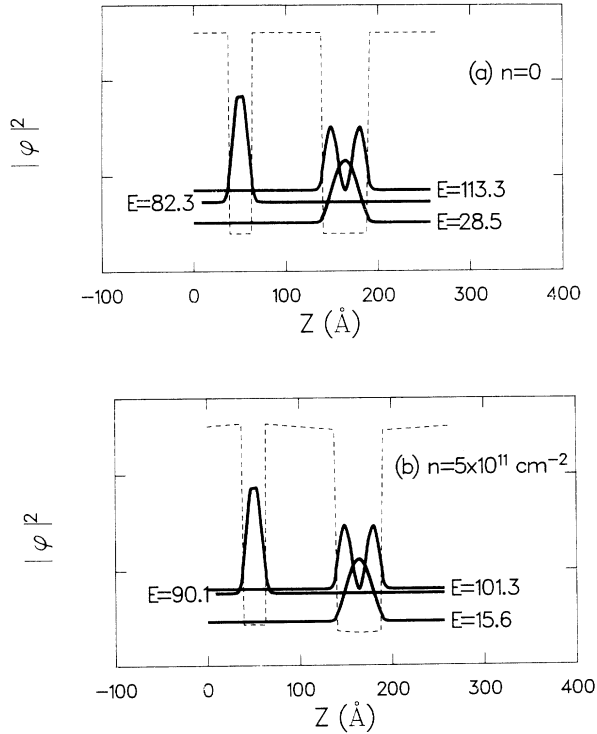
I. GALBRAITH, P. DAWSON, AND C. T. FOXON

FIG. 5. Band alignments of the heavy-hole subband edges showing the influence of the space-charge field set up by the electron-hole plasma for (a) $n = 0$ and (b) $n = 5 \times 10^{11}$ cm^2. The energies are in meV.

FIG. 6. Absorption spectra around the 68-Å QW band gap in the $L_n = 25$ Å, $L_b = 103$ Å, $L_W = 68$ Å sample at various pump intensities. The spectra have been offset vertically for clarity. The pump energy is 1.95 eV, i.e., above the 25-Å QW band gap.

calculations. We have checked that this is accurate to better than 1 meV for our structures.

For the sample with the 42-Å barrier, we find only a small amount of bleaching for the same pump powers as in Fig. 2, and essentially no shift of either resonance (not shown, see Ref. 6). This is consistent with there being a lower equilibrium carrier density in the 42-Å barrier sample than in the 76-Å barrier sample for the same pump power density. This we believe is because the hole tunneling time is shorter, enabling holes excited in the 25-Å well to get into the 50-Å well more easily and rapidly recombine. Consistent with this argument is the fact that we were not able to see any bleaching whatsoever at these power densities in the 25-Å barrier sample, where the tunneling time will be further reduced, leading to a lower equilibrium carrier density.

Following this investigation of the initial set of samples, a second set was specified to avoid the hole states being brought into resonance by the space-charge field. In this second set the quantum wells were specified to be 25 and 68 Å, so that the $n = 2$ heavy-hole subband edge of the wide well lies below the $n = 1$ heavy-hole subband edge of the narrow well. So the effect of the space-charge field will be to push the states further apart instead of bringing them into resonance. Care was also taken to ensure that none of the light-hole states could be brought into resonance by the space-charge field. Also, in this second set of samples, the barrier thickness was increased
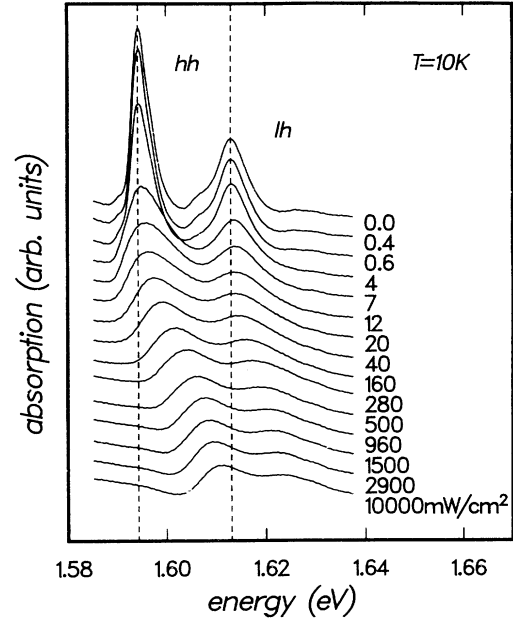
compared with the first set to enable the nonlinearities to be observed at even lower pump power densities. The barrier thicknesses were specified to be 76, 84, 93, and 103 Å.

To illustrate that we have achieved both of our aims in this new set, we show in Fig. 6 the 10-K cw pump-probe absorption spectrum from the sample with the 103-Å AlAs barriers. Quite clearly, we observe optical nonlinearities at ultralow pump power densities. We see a clear reduction in the strength of the $n = 1$ heavy-hole exciton in the 68-Å quantum well at a pump power density of only 0.6 mW/cm^2. Furthermore, at the highest pump power density used, we have been able to shift the heavy-hole resonance by 16 meV. The other samples in this set showed similar behavior in that similarly large shifts and strong bleaching of the exciton resonances could be achieved, the only systematic difference being that as the barrier thickness was reduced the pump power density required to produce equivalent changes in the nonlinear spectra increased.

To characterize this behavior, we show in Table I the pump power density required to reduce the strength of the $n = 1$ exciton peak of the 68-Å quantum well by 50%. Quite clearly, the exciton bleaching is more easily achieved as the AlAs barrier thickness is increased. We believe this is due to the increased equilibrium carrier density per unit input power due to the longer carrier lifetime caused by increase in the heavy-hole tunneling times as the barrier thickness is increased. This behavior is clearly illustrated if we examine the dynamics of the nonlinearity as shown in Fig. 7. In this figure we show the recovery of the transmission spectrum at the peak of the
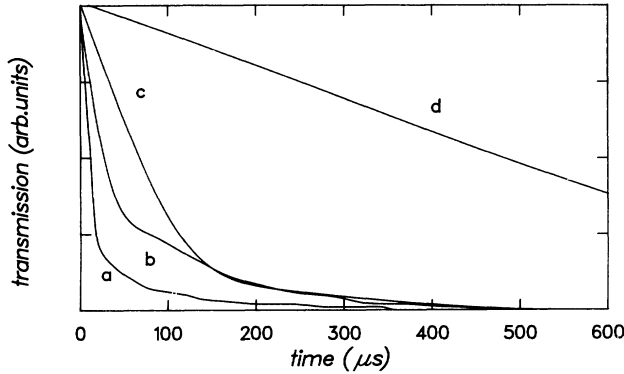
FIG. 7. Recovery of the transmission after switching off the pump in the four samples. (a) 103-Å barrier, (b) 93-Å barrier, (c) 84-Å barrier, and (d) 76-Å barrier. $T = 10$ K.

heavy-hole exciton resonance of the 68-Å quantum well following pulsed excitation. The power of the pulsed pump source was adjusted such that the exciton absorption peak was reduced by 50% at the end of the pulse. The gate of the boxcar was then scanned to monitor the recovery of the partially bleached exciton absorption peak. Clearly, this experiment reflects the decay of the spatially separated electron-hole population which we believe to be governed by the heavy-hole tunneling time. Unfortunately, these decay curves cannot be used to accurately measure the heavy-hole tunneling time, as we do not know the precise form of the change in the absorption spectrum with varying carrier density. It is also not possible for us to exclude the effects of any nonradiative processes which could affect these measurements. Nevertheless we can clearly see in the samples studied an increase in the recovery time as the barrier thickness increases in the different samples. This we believe reflects the increase in the heavy-hole tunneling time as the barrier thickness is increased. Quantitative support for this conclusion is provided if we take the experimentally determined curves and measure the time $(t_{1/2})$ for the transmission to recover by 50%. The values from the different barrier thicknesses are listed in Table I. Also shown in Table I are values for the heavy-hole tunneling times extrapolated from the calculations of Yu, Jackson, and McGill[28] using the measured XRD barrier thicknesses. Both the measured and theoretical times fall off exponentially with barrier thickness and lie in the same time regimes. Bearing in mind that the calculations were performed for a somewhat different structure from ours, the differences are not unexpected.

B. High-temperature results

In this subsection, we report on the results of pump-probe experiments on the samples with the 68-Å quantum wells in the temperature range 50–300 K. It would clearly be impossible to present all the data from all the samples over this temperature range, so we present only data from one sample that are representative of two types of behavior that we observed. For this purpose, we re-
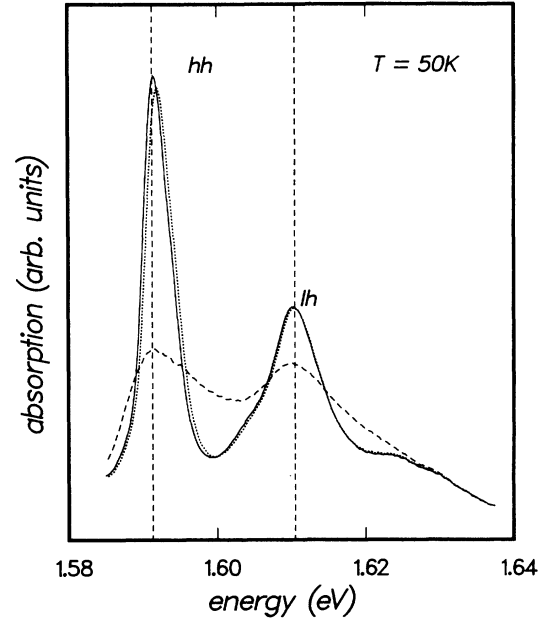

FIG. 8. Absorption spectra around the 68-Å QW band gap in the $L_n = 25$ Å, $L_b = 103$ Å, $L_W = 68$ Å sample at 50 K. Zero pump intensity (solid), pump tuned above the 25-Å QW band gap (dashed), and pump tuned below the 25-Å QW band gap (dotted).

port data from the sample with the nominally 103-Å-thick AlAs barrier. In Fig. 8 we show the results of pump-probe spectroscopy at 50 K with pump energies at 1.963 and 1.845 eV which lie above and below the 25-Å quantum-well gap, respectively. These experiments were performed with a pump power density of 100 mW/cm^2 and are compared with the zero pump power absorption spectrum. The main observations from these spectra are that we are still able to produce low power nonlinearities in the absorption spectrum of the 68-Å-thick quantum well by pumping above the gap of the 25-Å quantum well, thus generating a spatially separated electron-hole plasma. The major difference in the optical nonlinearity observed at this higher temperature compared with the data taken at 10 K is that, at this pump power density and even higher, we are not able to produce any significant blueshift of the exciton absorption peaks. A similar behavior has been reported[22] in type-II quantum wells and attributed to reduced band filling at the higher temperature.

We are able to observe significant nonlinearities in the absorption spectrum of the wider quantum well due to a spatially separated electron-hole plasma at temperatures up to about 200 K. Above this temperature a significant change occurs, as illustrated in Fig. 9. In this figure, we show the results of pump-probe experiments at 250 K at a power density of 400 mW/cm^2 when pumping at 1.894 and 1.776 eV, i.e., again above and below the 25-Å quantum-well gap. At this temperature the observed bleaching is much less than that observed at the lower temperatures, and it occurs whether we pump above or below the 25-Å quantum-well gap. We can attribute this behavior to a combination of several effects. The lifetime
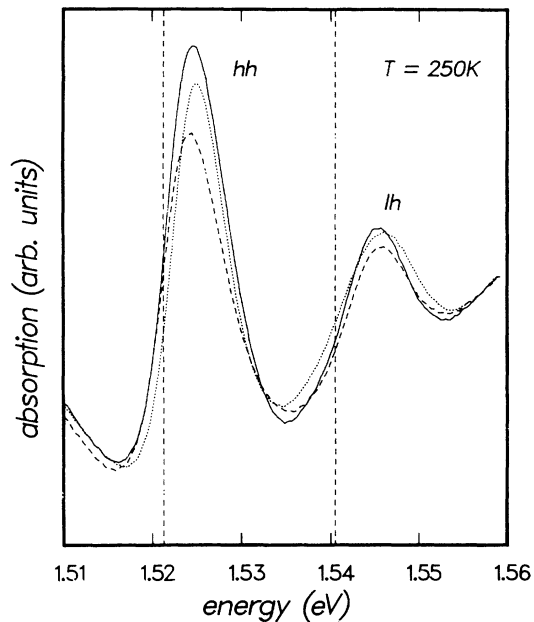
I. GALBRAITH, P. DAWSON, AND C. T. FOXON

FIG. 9. As Fig. 8 but at 250 K.

FIG. 10. Calculated absorption spectra around the 68-Å QW band gap at various densities. The spectra have been offset vertically for clarity.

of the spatially separated carriers is likely to decrease due to a combination of the following effects: (a) increased nonradiative recombination, (b) thermal excitation of holes out of the 25-Å quantum well and subsequent recombination in the 68-Å well, and (c) as predicted by Yu, Jackson, and McGill, it is anticipated that the average heavy-hole tunneling time will decrease with increasing lattice temperature.

Furthermore, it is well known that at these high temperatures the main recombination mechanism is dominated by free-carrier effects which can (at sufficiently low doping levels) lead to carrier decay times in excess of hundreds of nanoseconds.[9] In fact, the decay time of luminescence from the 68-Å quantum well was measured to be 170 ns. This decay time is sufficiently long to allow a significant electron *and* hole density to be directly excited in the 68-Å quantum well to produce the small exciton bleaching we observe. So at temperatures above 200 K recombination in the 68-Å well occurs on a time scale similar to the hole tunneling time and hence carriers directly excited in the 68-Å well make a significant contribution to the equilibrium density.

C. Calculated absorption spectra

We turn now to the results of the calculations of the absorption spectra obtained from the inhomogeneously broadened solutions of Eq. (3). We used a homogeneous linewidth of 1 meV and required a standard deviation of the well width of 2 Å to fit the linear spectrum. This variation is less than one monolayer. The exact value required to fit the linear spectrum varies somewhat from sample to sample. As shown in Fig. 10, the calculations reproduce qualitatively the main features seen in the experiments, namely an initial bleaching with no shift in both the heavy- and light-hole exciton peaks. At higher
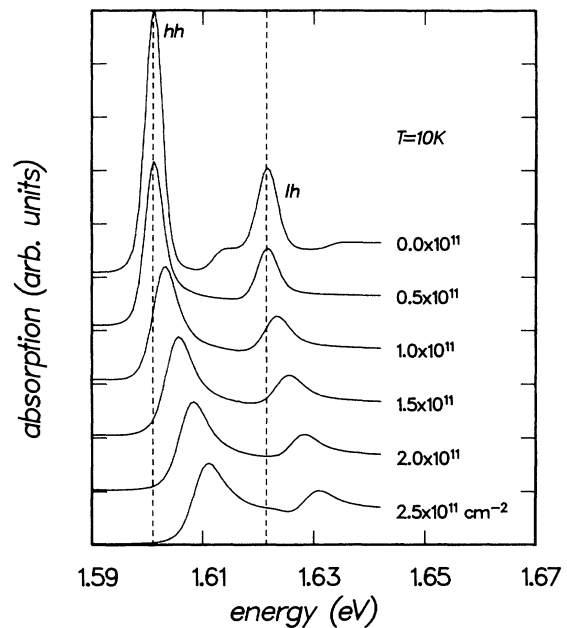
densities, both peaks shift to higher energy as the filling of the bands begins to become appreciable. As in the type-II case there is no gain even at the highest densities. In contrast to the type-II case, however, the behavior of the light hole is to shift to higher energy and bleach simultaneously with the heavy hole. The difference arises because, in the mixed type-I–type-II structures, both the $n = 1$ heavy- and light-hole states are unoccupied, whereas in the type-II materials the heavy hole is occupied but the light hole is empty.

The heavy-hole–light-hole exciton splitting remains practically constant in the calculations. Experimentally this splitting is found to decrease with increasing intensity. We attribute this to the effect of the nonparabolic
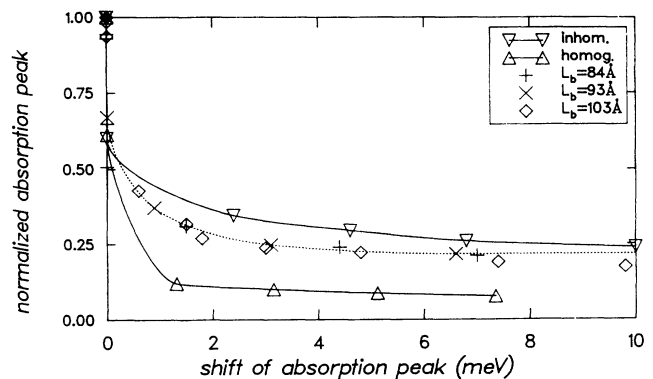

FIG. 11. Change in absorption vs exciton energy shift showing experimental results from three samples. Theoretical points with and without inhomogeneous broadening are also shown. The temperature is 10 K.

valence bands. As the carrier density increases, the absorption peak is pushed further from $k = 0$ and towards the anticrossing of the heavy- and light-hole bands. Hence the heavy-hole–light-hole splitting decreases.

In order to obtain a more quantitative comparison between theory and experiment we plot in Fig. 11 the normalized heavy-hole absorption strength versus exciton shift. We show both the experimental points for three samples and several theoretical curves which we discuss below. It is notable that the points for all three samples lie essentially on one curve. This gives us some confidence that only the equilibrium carrier density is changing between samples for a given pump intensity.

If, in the calculations, inhomogeneous broadening is neglected (Fig. 11), the bleaching occurs very rapidly before any appreciable shift in the peak. The influence of the inhomogeneous broadening is to reduce the amount of bleaching. This is due primarily to the broadening of the linear spectrum leading to a reduction of the peak height. At higher densities the calculated homogeneous spectra are found to be insensitive to the value of γ used.

This conclusion on the influence of inhomogeneous broadening applies equally well to the bleaching caused by the quantum-confined Stark effect. However, since one usually works with somewhat wider quantum wells than we have here (typically 100 Å), the effects will be somewhat less.

V. CONCLUSIONS

In conclusion we have demonstrated optical nonlinearities at ultralow pump power densities in a range of quantum-well structures. At low temperatures ($T = 10$ K) we were able to set up a long-lived spatially separated electron-hole plasma by allowing electrons created in a narrow well to thermalize to a wider well, whereas the heavy holes were prevented from tunneling to the wide well by the large barrier thicknesses involved. We have shown that the pump power densities and the dynamics of the exciton bleaching phenomena are strong functions of barrier thickness and are almost certainly governed by the heavy-hole tunneling rates. This behavior was observed at temperatures up to 200 K, above which we were unable to see any large effects due to a spatially separated electron-hole plasma. The precise reasons for this behavior are not yet clear and require further study. Theoretical modeling of the observed nonlinearities, based on the semiconductor Bloch equations, provide a quantitatively accurate description of the band-edge nonlinearities.

Clearly, the mixed type-I–type-II structure could prove a useful addition to the range of low-dimensional structures that it is now possible to grow with modern epitaxial growth techniques. In the future it should allow us to study various physical phenomena such as hole tunneling, spatial electron scattering, and the thermal excitation of carriers out of quantum wells.

[1]*Optical Nonlinearities and Instabilities in Semiconductors*, edited by H. Haug (Academic, London, 1988).

[2]H. Haug and S. W. Koch, *Quantum Theory of Electronic and Optical Properties of Semiconductors* (World Scientific, Singapore, 1990).

[3]S. Schmitt-Rink, D. S. Chemla, and D. A. B. Miller, Adv. Phys. **38**, 89 (1989).

[4]D. A. B. Miller, Opt. Quantum Electron. **22**, S61 (1990).

[5]P. Dawson, I. Galbraith, A. I. Kucharska, and C. T. Foxon, Appl. Phys. Lett. **58**, 1991.

[6]P. Dawson, I. Galbraith, A. I. Kucharska, and C. T. Foxon, Proc. SPIE **1362**, 385 (1991).

[7]J. Feldmann, J. Nunnenkamp, G. Peter, E. Göbel, J. Kuhl, K. Ploog, P. Dawson, and C. T. Foxon, Phys. Rev. B **42**, 5809 (1990).

[8]J. Feldmann, G. Peter, E. O. Göbel, P. Dawson, K. J. Moore, C. T. Foxon, and R. J. Elliot, Phys. Rev. Lett. **59**, 2337 (1987).

[9]H.-C. Lee, A. Kost, M. Kawase, A. Hariz, P. D. Dapkis, and E. M. Garmire, IEEE J. Quantum Electron. **QE-24**, 1581 (1988).

[10]S. H. Park, J. F. Morhange, A. D. Jeffery, R. A. Morgan, A. Chavez-Pirson, H. M. Gibbs, M. Derstine, A. C. Gossard, J. H. English, and W. Wiegmann, Appl. Phys. Lett. **52**, 1201 (1988).

[11]N. Peyghambarian, H. M. Gibbs, J. L. Jewell, A. Antonetti, A. Migus, D. Hulin, and A. Hysyrowicz, Phys. Rev. Lett. **53**, 2433 (1984).

[12]A. Mysyrowicz, D. Hulin, A. Antonetti, A. Migus, D. Hulin, W. T. Masselink, H. Morkoc, H. M. Gibbs, and N. Peyghambarian, Phys. Rev. Lett. **56**, 4389 (1986).

[13]C. Weber, C. Klingshirn, D. S. Chemla, D. A. B. Miller, J. E. Cunningham, and C. Ell, Phys. Rev. B **38**, 12 748 (1988).

[14]K.-H. Schlaad, C. Weber, J. E. Cunningham, C. V. Hoof, G. Borghs, G. Weimann, W. Schlapp, H. Nickel, and C. Klingshirn, Phys. Rev. B **43**, 4268 (1991).

[15]M. Lindberg and S. W. Koch, Phys. Rev. B **38**, 3342 (1988).

[16]H. Haug and S. Schmitt-Rink, Prog. Quantum Electron. **9**, 3 (1984).

[17]W. Schäfer, R. Binder, and K. H. Schuldt, Z. Phys. B **70**, 145 (1988).

[18]C. Ell, R. Blank, S. Benner, and H. Haug, J. Opt. Soc. Am. B **6**, 2006 (1989).

[19]A. M. Fox, D. A. B. Miller, G. Livescu, J. E. Cunningham, J. E. Henry, and W. Y. Jan, Appl. Phys. Lett. **57**, 2315 (1990).

[20]G. R. Olbright, W. S. Fu, A. Owyoung, J. F. Klem, R. Binder, I. Galbraith, and S. W. Koch, Phys. Rev. Lett. **66**, 1358 (1991).

[21]J. Feldmann, E. Göbel, and K. Ploog, Appl. Phys. Lett. **57**, 1520 (1990).

[22]G. R. Olbright, W. S. Fu, J. F. Klem, H. M. Gibbs, G. Khitrova, R. Pon, B. Fluegel, K. Meissner, N. Peyghambarian, R. Binder, I. Galbraith, and S. W. Koch, Phys. Rev. B **44**, 3043 (1991).

[23]T. Mishina, F. Sasaki, and Y. Matsumoto, J. Phys. Soc. Jpn.

59, 2635 (1990).

[24]H. W. van Kesteren, E. C. Cosman, P. Dawson, K. J. Moore, and C. T. Foxon, Phys. Rev. B **39**, 13 426 (1989); P. Dawson, C. T. Foxon, and H. W. van Kesteren, Semicond. Sci. Technol. **5**, 54 (1990).

[25]R. Binder, I. Galbraith, and S. W. Koch, Phys. Rev. B **44**, 3031 (1991).

[26]G. Olbright, J. Klem, A. Owyoung, T. M. Brennen, R. Binder, and S. W. Koch, J. Opt. Soc. Am. B **7**, 1473 (1990).

[27]See, for example, G. Bastard, *Wave Mechanics Applied to Semiconductor Heterostructures* (Les Editions de Physique, Paris, 1989).

[28]E. T. Yu, M. K. Jackson, and T. C. McGill, Appl. Phys. Lett. **55**, 744 (1989).